creating tear points, although this bias needs to be quantified in actualistic studies.
21. *Corylites* and *Alnus* fit well with the resource availability hypothesis [P. D. Coley, J. P. Bryant, F. S. Chapin III, *Science* **230**, 895 (1985)] in which high herbivory rates are correlated with short leaf lifespan (*Corylites* and *Alnus* were deciduous), high growth rates and relatively early successional status (*Corylites* and *Alnus* had tiny, wind- or water-dispersed fruits and colonized disturbed environments on floodplains), and low concentrations of defensive compounds (implied).
22. G. Bond, in *Symbiotic Nitrogen Fixation in Plants*, P. S. Nutman, Ed. (Cambridge Univ. Press, Cambridge, 1976), pp. 443–474; C. P. Onuf, J. M. Teal, I. Valiela, *Ecology* **58**, 514 (1977); W. J. Mattson Jr., *Annu. Rev. Ecol. Syst.* **11**, 119 (1980); R. E. Ricklefs and K. K. Matthew, *Can. J. Bot.* **60**, 2037 (1982); J. J. Furlow, in *Magnoliophyta: Magnoliidae and Hamamelidae,* vol. 3 of *Flora of North America*, Flora of North America Editorial Committee, Ed. (Oxford Univ. Press, New York, 1997), pp. 507–538. Phylogenetic analysis of DNA sequences from the *rbcL* gene places all actinorhizal plants within a single clade, indicating that actinorhizal association is ancient [D. E. Soltis *et al., Proc. Natl. Acad. Sci. U.S.A.* **92**, 2647 (1995)].
23. Insect damage on the single dicot species that was abundant in both samples (*Averrhoites affinis*) increased from five types in the Paleocene to nine in the Eocene (Fig. 5).
24. Although the most specialized damage types are rare, sampling was intensive (*10*, *14*), which supports our view that the inferred turnover of herbivores is not a sampling artifact. The percentages listed should be regarded as minima given the difficulty of evaluating the more generalized feeding groups.
25. S. L. Wing, H. Bao, P. L. Koch, in *Warm Climates in Earth History*, B. T. Huber, K. MacLeod, S. L. Wing, Eds. (Cambridge Univ. Press, Cambridge, 1999), pp. 197–237.
26. R. N. Coulson and J. A. Witter, *Forest Entomology: Ecology and Management* (Wiley, New York, 1984).
27. P. Wilf, *Paleobiology* **23**, 373 (1997).
28. L. J. Webb, *J. Ecol.* **47**, 551 (1959). The logarithmic mean area was used for each Webb category to estimate total leaf area [P. Wilf, S. L. Wing, D. R. Greenwood, C. L. Greenwood, *Geology* **26**, 203 (1998)].
29. We thank A. Ash, R. Schrott, K. Werth, and others for field and laboratory assistance, Western Wyoming Community College for logistical support, and W. DiMichele, P. Dodson, R. Horwitt, B. Huber, S. Wing, and two anonymous reviewers for helpful comments on the manuscript. P.W. was supported by Smithsonian Institution predoctoral and postdoctoral fellowships, the Smithsonian's Evolution of Terrestrial Ecosystems Program (ETE), a University of Pennsylvania Dissertation Fellowship, the Geological Society of America, Sigma Xi, and the Paleontological Society. C.C.L. was supported by the Walcott Fund of the National Museum of Natural History. This is ETE contribution number 68.

19 March 1999; accepted 5 May 1999

On the Weakening Relationship Between the Indian Monsoon and ENSO

K. Krishna Kumar,[1]*† Balaji Rajagopalan,[2] Mark A. Cane[2]

Analysis of the 140-year historical record suggests that the inverse relationship between the El Niño–Southern Oscillation (ENSO) and the Indian summer monsoon (weak monsoon arising from warm ENSO event) has broken down in recent decades. Two possible reasons emerge from the analyses. A southeastward shift in the Walker circulation anomalies associated with ENSO events may lead to a reduced subsidence over the Indian region, thus favoring normal monsoon conditions. Additionally, increased surface temperatures over Eurasia in winter and spring, which are a part of the midlatitude continental warming trend, may favor the enhanced land-ocean thermal gradient conducive to a strong monsoon. These observations raise the possibility that the Eurasian warming in recent decades helps to sustain the monsoon rainfall at a normal level despite strong ENSO events.

Most parts of India receive a major proportion of their annual rainfall during the summer (June to September) monsoon season. Extreme departures from normal seasonal rainfall, such as large-scale droughts and floods, seriously affect agricultural output and regional economies. By the early 1900s, investigators had identified the two large-scale forcings still thought to be most important for predicting monsoon anomalies: Himalayan/Eurasian snow extent (*1*) and the ENSO cycle (*2*). The former is generally believed to provide an indication of the premonsoon thermal condition over the Asian land mass. Warmer conditions are thought to aid the buildup of a strong land-sea thermal gradient during the summer (*3, 4*). ENSO, the largest known climatic forcing of interannual monsoon variability, acts through the east-west displacement of large-scale heat sources in the tropics (*5*). Numerous studies (*6*) have shown a significant simultaneous association between the monsoon rainfall over India and ENSO indices. However, secular variations in the relationships between monsoon rainfall and its predictors have also been noted (*7*). These variations have been found to be linked to changes in ENSO characteristics such as amplitude and period (*8*).

Almost all the statistical seasonal prediction schemes of monsoon rainfall rely heavily on the change in magnitude in various ENSO indices (*8, 9*) from winter [December to February (DJF)] to spring [March to May (MAM)]. Numerical general circulation models (GCMs) are also used for seasonal rainfall prediction. The monsoon simulated in these GCMs is more sensitive to the sea surface temperatures (SSTs) specified in the Pacific (*10*) than to other external boundary forcings. Hence, the success of seasonal forecasts of monsoon rainfall depends on the stationarity of the monsoon-ENSO relationship.

We used data on Indian monsoon rainfall, SST, velocity potential fields, and global surface temperatures (*11*) to examine the simultaneous relationship between the monsoon and ENSO during the last 142 years, and to explore possible roles for other climatic forcings.

Low-frequency variations in the monsoon rainfall and a widely used measure of ENSO, the NINO3 index (*11*), show a clear resemblance until the late 1970s (Fig. 1A), but diverge thereafter. This change reflects the recent modest increase in the monsoon rainfall despite an increase in the magnitude and frequency of ENSO warm events. Sliding correlations on a 21-year moving window between monsoon rainfall and the NINO3 index are strong during the entire data period with the exception of the recent two to three decades (Fig. 1B), not withstanding the considerable impact of the 1982 and 1987–88 ENSO events on the monsoon. The drop in correlations in the recent decades is found to be significant on the basis of bootstrap confidence limits (*12*). The loss of monsoon-ENSO correlation is not particular to NINO3, but appears with any ENSO index. Correlation patterns of monsoon rainfall with SSTs in the Pacific show a coherent region of strong correlations in the central and eastern equatorial Pacific before 1980 and no region with statistically significant correlations thereafter.

The conventional description of the ENSO-induced teleconnection response in the monsoon is through the large-scale east-west shifts in the tropical Walker circulation. During an El Niño event, the tropical convection and the associated rising limb of the Walker circulation normally located in the western Pacific shift toward the anomalously

[1]International Research Institute (IRI) for Climate Prediction, Lamont-Doherty Earth Observatory (LDEO) of Columbia University, Post Office Box 1000, Route 9W, Palisades, NY 10964–8000, USA. [2]LDEO of Columbia University, Post Office Box 1000, Route 9W, Palisades, NY 10964–8000, USA.

*Permanent address: Indian Institute of Tropical Meteorology, Dr. Homi Bhabha Road, Pashan, Pune 411008, India.

†To whom correspondence should be addressed. E-mail: krishna@iri.ldeo.columbia.edu

warm waters in the central and eastern Pacific. Consequently, there is an anomalous subsidence extending from the western Pacific region to the Indian subcontinent. This subsidence suppresses convection and precipitation over the western Pacific and the Indian subcontinent. It is associated with anomalously high pressure over the western Pacific–eastern Indian Ocean sector and anomalously low pressure over the eastern and central Pacific. Walker (*2*) long ago recognized that these pressure oscillations could profoundly influence the monsoon circulation and rainfall over India. Numerous observational studies since then have noted this connection (*6*), and GCM simulations have reproduced it (*13*).

The correlations between the monsoon rainfall and 200-hPa velocity potential, a good surrogate for the "Walker circulation," are strong in the period 1958–80 and weaken appreciably during 1981–97 (Fig. 2, A and B), a period of reduced monsoon variability even while ENSO variability was strong. This would suggest a reduction in the strength of ENSO-induced subsidence in the western Pacific–eastern Indian ocean sector.

To examine the connection between ENSO and subsidence, we computed El Niño year composites of velocity potential anomalies at 200 hPa during summer. The composites corresponding to the El Niño events of 1958–80 (Fig. 2C) show anomalous subsidence (positive values) over south Asia and southeast Asia and also over northern and northeastern parts of South America. The center of anomalous rising motion (negative values) is located in the central Pacific, around 150°W. The composite fields of recent (1981–97) El Niño events (Fig. 2D) show a significant southeastward shift in the centers of anomalous subsidence and rising motion. Similar results but with an opposite sign were obtained from the composites of anomalies at 850 hPa. There is more subsidence (less rainfall) over southern Indonesia and northwest Australia and less subsidence (relatively more rainfall) over the Indian region. During the strong 1997 El Niño, Indonesia had severe drought while the monsoon rainfall over India was normal (+2% of the long-term mean). Note that the South American cell of subsidence in the earlier period is replaced by rising motion in the recent period.

The fundamental mechanism of the monsoon is the land-sea thermal contrast (*3*–*5*). The 19th-century discovery of an inverse relation between Himalayan winter and spring snow accumulation and following summer monsoon rainfall over India (*1*) has been substantiated by numerous studies of snow cover over a wide region covering Eurasia (*14*). Modeling studies (*15, 16*) provide corroborating evidence. The physical mechanisms underlying the snow cover–monsoon rainfall relationships are explained as follows. Increased albedo due to higher snow cover means less solar radiation is absorbed at the surface. Also, more solar energy is consumed in melting the excess snow mass during the spring, resulting in a smaller surface temperature rise. The excess melt water subsequently increases soil moisture, which continues to reduce the heating of the ground even after the snow melt. The land and overlying atmospheric column will be colder than normal, reducing the spring and summer land-sea contrast needed to initiate and sustain a strong monsoon.

Snow cover data only exists from 1973 onward. However, there is a close relationship between snow cover extent and the surface temperatures over the Northern Hemisphere (*17*), in particular Eurasia (*18*). Also, Northern Hemispheric surface temperatures during January and February have been shown to be positively correlated with the following summer monsoon rainfall (*19*). We will use the long record of surface temperatures over Eurasia as a proxy for snow extent.

The difference between composites of winter Eurasian surface temperatures preceding the El Niño events of 1981–97 and those of 1951–80 (Fig. 3A) shows that surface temperatures were considerably warmer during recent El Niño events. The spring season temperature differences are somewhat smaller, but similar. This difference in the El Niño composites of winter surface temperatures (Fig. 3A) is quite similar to the difference in the winter climatologies of these two periods (Fig. 3B), indicating that the El Niño year differences are a part of the general increase in the surface temperatures over the continental mid-latitude regions in winter and spring (*17*). This may also indicate the possibility that the changes in ENSO activity and Eurasian warming in the recent period may be linked (*20*).

The explanation outlined above for a connection between Eurasian temperature and monsoon strength may account for the behavior observed in recent decades. In El Niño events before 1980, colder Eurasian temperature anomalies coupled with positive SST anomalies in the Pacific coincided with negative monsoon rainfall anomalies over India. The usual historical inverse relation between the monsoon and ENSO was maintained. In recent decades, the increased premonsoon surface temperatures over Eurasia far exceeded the warming in the Indian Ocean. Thus, the stronger land-sea thermal gradient conducive for a strong monsoon was favored, apparently overriding the influence of El Niño. This increase in the Eurasian surface temperatures coupled with the observed southeastward shift of the tropical convection associated with recent El Niño events may help maintain the monsoon at its normal strength despite stronger ENSO events in the recent period.

To better isolate the role of Eurasian temperature anomalies in the performance of the Indian monsoon, we composited winter temperatures from strong and weak monsoon years from 1871 to 1997 (Fig. 3, C and D). Regardless of ENSO state, the expected connection appears: a strong monsoon coincides with warmer temperatures over Eurasia. This holds even if the post-1980 warm period is excluded, though the Eurasian warming is weaker.

If we categorize the years based on Eurasian temperatures and look at the difference in monsoon strength, the signal is in the expected sense but weak. The ENSO influence was strong enough to induce a weak monsoon in many of the years when Eurasian temperatures were warm. However, the recent Eurasian warming is larger than was typical in the past and may now be able to consistently overcome the negative influence of ENSO warm events.

The enhanced Eurasian surface temperatures in the recent period is part of a global warming trend. It is possible (perhaps even likely), but not certain, that this warming trend results from anthropogenic effects (*17*). Some recent coupled ocean-atmosphere model studies (*21*) have suggested an intensification of the Asian summer monsoon rainfall with increased atmospheric greenhouse gas concentrations. This increase in the monsoon

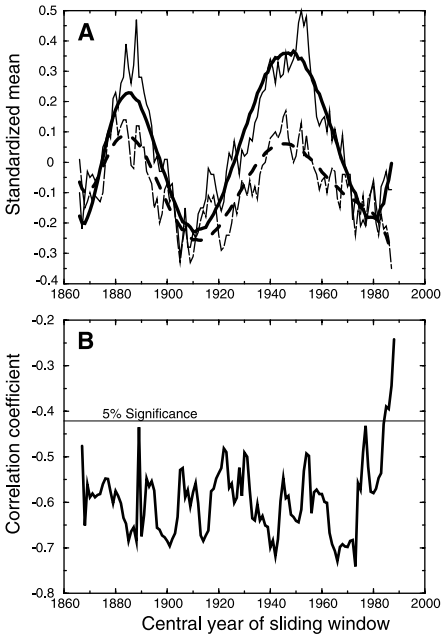

Fig. 1. (**A**) Shown are 21-year sliding standardized means of Indian summer monsoon rainfall (thin line) and June to August (JJA) NINO3 SST anomalies (thin dashed line) during 1856–1997. The corresponding solid lines represent the smoothed values (smoothing is done by fitting a polynomial). The sign of NINO3 SST is reversed to facilitate direct comparison. (**B**) Shown are 21-year sliding correlations between Indian summer monsoon rainfall and NINO3 SST anomalies (JJA) during 1856–1997. The horizontal line shows the 5% significance level.

rainfall over the Indian region has been attributed to the enhanced land-sea thermal gradient as a result of the greater warming over land compared to the tropical oceans (*21*).

Given the lack of upper air data, it is difficult to know whether the southeastward shift in the Walker circulation occurred at any time before 1950. In fact, we cannot entirely rule out the possibility that it is an artifact of changes in data coverage. Explanations for the shift are highly speculative. One possibility that can be tested in careful model experiments is that the warming of the tropical oceans has expanded the western Pacific region above 28°C to the east and south, causing the

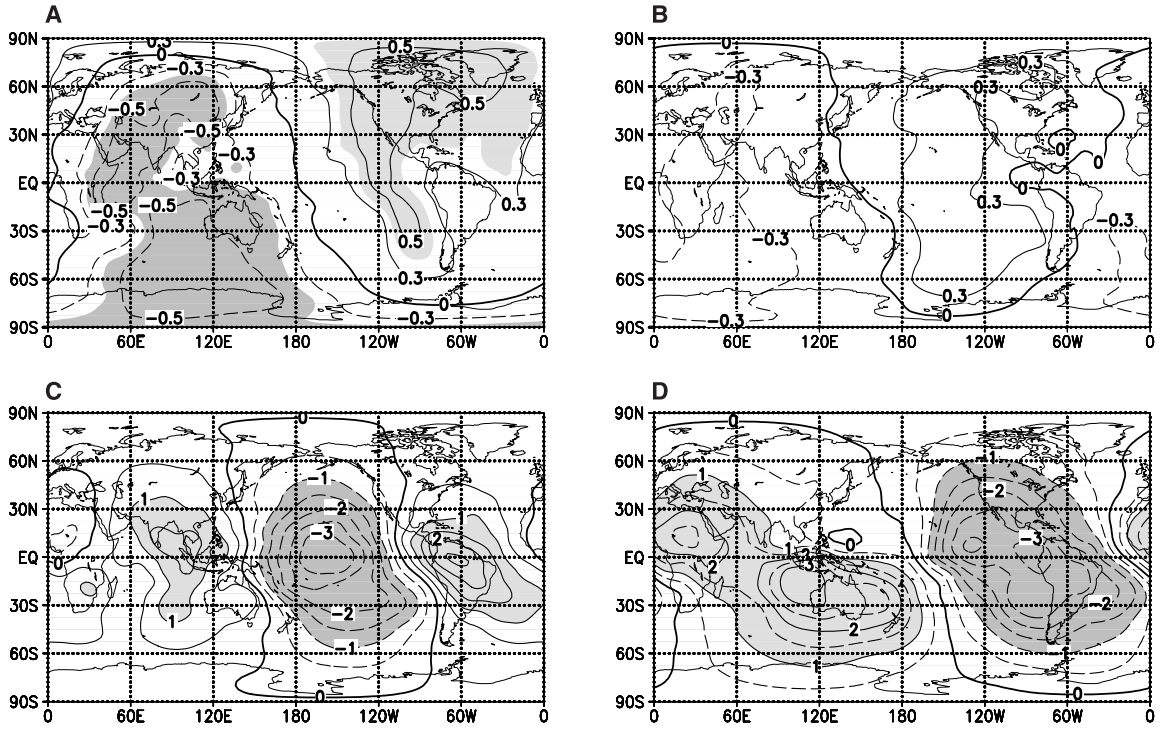

Fig. 2. Correlation between monsoon rainfall and velocity potential at 200 hPa (**A**) during 1958–80 and (**B**) 1981–1997. Correlations significant at 5% and above are shaded. Panels (C) and (D) show composites of summer velocity potential ($\times 10^5$) at 200 hPa for the El Niño events during (**C**) 1958–80 and (**D**) 1981–97. The El Niño years were identified by NINO3 SST anomalies during autumn and winter seasons exceeding one standard deviation.

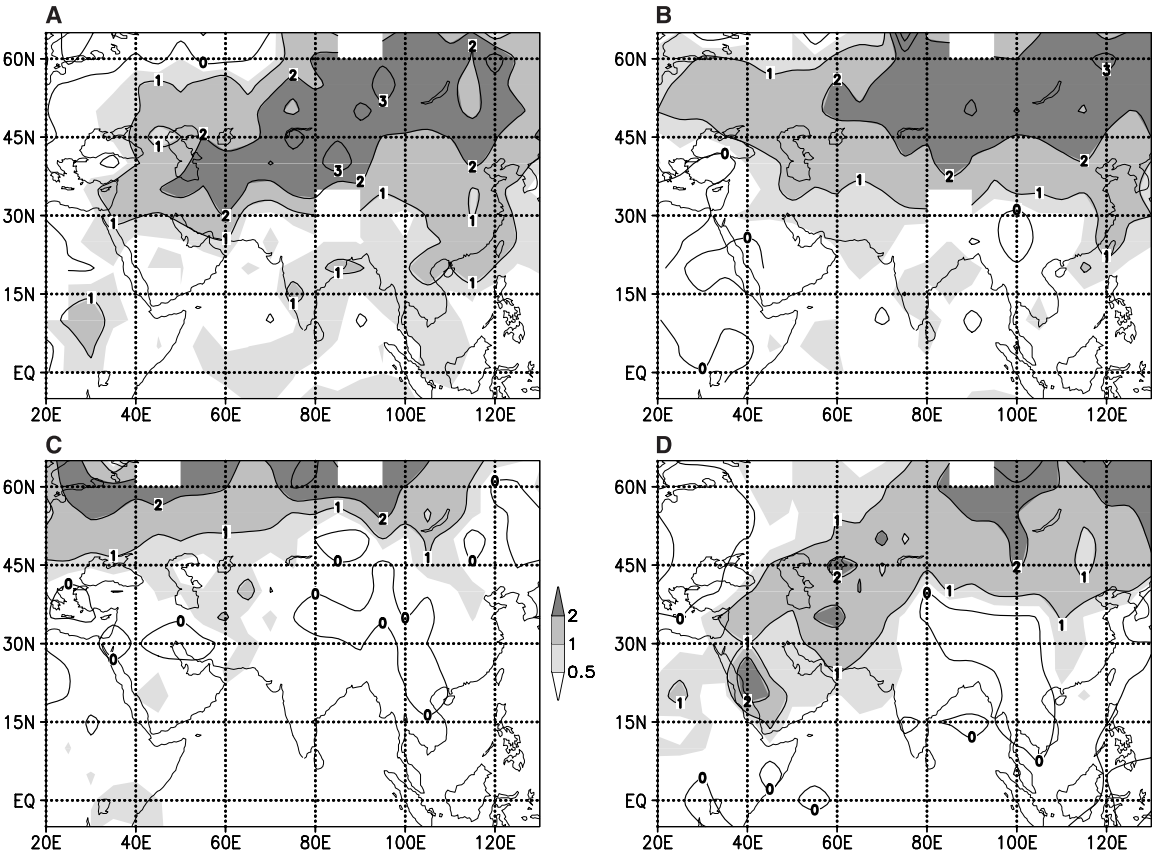

Fig. 3. Winter (DJF) surface temperature difference between (**A**) composites of El Niño events during 1981–97 and 1871–1980, (**B**) climatologies of 1981–97 and 1871–1980, (**C**) strong and weak monsoon years during 1871–1997, and (**D**) strong and weak monsoon years in warm ENSO events during 1871–1997. Strong and weak monsoon years were identified by rainfall exceeding $\pm 1\sigma$ respectively, except in (D), where strong monsoon years are those exceeding the long-term average.

convective center to also move to the southeast. Another possibility is that the warming of Eurasia and the consequent strengthening of the monsoon has effectively pushed the Walker cell further away, to the southeast. Again, this is hard to test with data but could be checked with sufficiently realistic models.

We suggest that both the shift in Walker circulation anomalies and the enhanced land-sea gradient are countering the historical monsoon-ENSO inverse relationship, keeping the monsoon at a normal level despite increased ENSO activity in the recent decades. This recent breakdown in the ENSO-monsoon connection is without precedent in the historical record. It is noteworthy that all the links we present are consistent with the idea that the root cause is the recent warming trend. This may all be because of natural variability, but there is the intriguing possibility that global warming has broken the link between ENSO and the monsoon by preventing monsoon failure.

References and Notes

1. H. F. Blanford, *Proc. R. Soc. London* **37**, 3 (1884).
2. G. T. Walker, *Q. J. R. Meteorol. Soc.* **22**, 223 (1918).
3. P. J. Webster *et al.*, *J. Geophys. Res.* **103**, 14451 (1998).
4. P. J. Webster, in *Monsoons*, J. S. Fein and P. L. Stephens, Eds. (Wiley, New York, 1987), pp. 275–332.
5. J. Shukla, in (*4*), pp. 399–464.
6. G. B. Pant and B. Parthasarathy, *Arch. Meteorol. Geophys. Bioklimatol. Ser. B* **29**, 245 (1981); E. M. Rasmusson and T. H. Carpenter, *Mon. Weather Rev.* **111**, 517 (1983); C. F. Ropelewski and M. S. Halpert, *ibid.* **115**, 1606 (1987).
7. B. Parthasarathy, K. Rupa Kumar, A. A. Munot, *J. Clim.* **4**, 927 (1991); K. Krishna Kumar, M. K. Soman, K. Rupa Kumar, *Weather* **50**, 449 (1995); V. Krishnamurthy and B. N. Goswami, *COLA Report No. 62* (Center for Ocean-Land-Atmosphere, Calverton, MD, 1998).
8. K. Krishna Kumar, R. Kleeman, M. A. Cane, B. Rajagopalan, *Geophys. Res. Lett.* **26**, 75 (1999).
9. J. Shukla and D. A. Paolino, *Mon. Weather Rev.* **111**, 1830 (1983); S. Hastenrath, *Climate Dynamics of the Tropics* (Kluwer Academic, Dordrecht, Netherlands, 1991).
10. K. R. Sperber and T. N. Palmer, *J. Clim.* **9**, 2727 (1996).
11. The following data sets were used in this study: (i) All-India summer (June to September) monsoon rainfall during 1856–1997 [B. Parthasarathy, K. Rupa Kumar, A. A. Munot, *Theor. Appl. Climatol.* **49**, 217 (1994); N. A. Sontakke, G. B. Pant, N. Singh, *J. Clim.* **6**, 1807 (1993)]. (ii) The equatorial Pacific (NINO3) SST anomalies during 1856–1997. NINO3 area (5°S-5°N and 150°W-90°W) SST anomalies were obtained from the grid-point data of A. Kaplan *et al.* [*J. Geophys. Res.* **103**, 18567 (1998)] for the era 1856–1949, and those during 1950–1997 are taken from the Climate Prediction Center, Washington, DC (http://nic.fb4.noaa.gov/data/cddb/). The correlation between the two NINO3 series during the common period of 1951–90 is 0.97. (iii) Monthly velocity potential at 200 hPa during 1958–97 were obtained from the NCEP/NCAR reanalysis [E. Kalnay *et al.*, *Bull. Am. Meteorol. Soc.* **77**, 437 (1996)]. (iv) The 5° by 5° surface temperature anomalies on land as well as oceans during 1871–1997 [P. D. Jones, *J. Clim.* **7**, 1794 (1994); D. E. Parker, C. K. Folland, M. Jackson, *Clim. Change* **31**, 559 (1995)]. The anomalies are with respect to the 1961–90 climatology.
12. The rainfall and the NINO3 series are resampled [B. Efron, *Ann. Stat.* **7**, 1 (1979)] 1000 times in random 21-year chunks. For each resample, the correlation between the rainfall and NINO3 series is computed. The 5th and 95th percentile of these 1000 correlation coefficients provide 95% confidence limits of −0.45 and −0.70, respectively. The correlations in the recent decades fall outside this range, indicating that the relationship in this period is significantly different from the rest of the record.
13. J. Ju and J. Slingo, *Q. J. R. Meteorol. Soc.* **121**, 1133 (1995); G. A. Meehl and J. M. Arblaster, *J. Clim.* **11**, 1356 (1998).
14. D. J. Hahn and J. Shukla, *J. Atmos. Sci.* **33**, 2461 (1976); S. Yang, *Int. J. Climatol.* **16**, 125 (1996); M. Shankar Rao, K. M. Lau, S. Yang, *ibid.*, p. 605.
15. T. P. Barnett, L. Dümenil, U. Schlese, E. Roeckner, M. Latif, *J. Atmos. Sci.* **46**, 661 (1989).
16. T. Yasunari, A. Kitoh, T. Tokioka, *J. Meteorol. Soc. Jpn.* **69**, 473 (1991); G. A. Meehl, *Science* **266**, 263 (1994); A. D. Vernekar, J. Zhou, J. Shukla, *J. Clim.* **8**, 248 (1995); X. Shen, M. Kimoto, A. Sumi, *J. Meteorol. Soc. Jpn.* **76**, 217 (1998).
17. N. Nicholls *et al.*, in *Climate Change 1995: IPCC Second Assessment*, J. T. Houghton *et al.*, Eds. (Cambridge Univ. Press, Cambridge, 1996), pp. 133–192.
18. A. Bamzai and J. Shukla, *COLA Report No. 53* (Center for Ocean-Land-Atmosphere, Calverton, MD, 1998).
19. R. K. Verma, K. Subramaniam, S. S. Dugam, *Proc. Indian Acad. Sci. (Earth Planet. Sci.)* **94**, 187 (1985).
20. Model simulations [A. Kumar, A. Leetmaa, M. Ji, *Science* **266**, 632 (1994)] reproduce the observed Eurasian warming in the recent decades when forced by global SSTs associated with strong and weak ENSO situations. However, the mechanisms for this link are not clear. A causal link in the opposite sense may also exist (*15*), where Eurasian snow cover anomalies may influence ENSO.
21. G. A. Meehl and W. M. Washington, *Science* **260**, 1101 (1993); B. Bhaskaran, J. F. B. Mitchell, J. R. Lavery, M. Lal, *Int. J. Climatol.* **15**, 873 (1995).

22. We thank C. Ropelewski, R. Kleeman, S. Zebiak, and Y. Kushnir for useful discussions and comments. Supported by National Oceanic and Atmospheric Administration (NOAA) grant NA67GP0299. B.R. and M.A.C. were partially supported by NOAA grant NA56GP0221. This is Lamont-Doherty Earth Observatory contribution 5937.

5 March 1999; accepted 11 May 1999

Gold Solubility in Supercritical Hydrothermal Brines Measured in Synthetic Fluid Inclusions

Robert R. Loucks[1]* and John A. Mavrogenes[1,2]

Dissolved gold contents in chloride brines that were experimentally saturated with gold, magnetite, iron sulfides, orthoclase, and muscovite at 550° to 725°C and 100 to 400 megapascals are reported here. Microsamples of the fluid were isolated at the experimental temperature and pressure as fluid inclusions in quartz. Individual fluid inclusions were opened by laser ablation and analyzed by inductively coupled plasma mass spectrometry. The results show that gold solubility as sulfide species in supercritical brines is far higher than previously supposed. Dissolved gases such as molecular hydrogen sulfide that are ineffective metal-complexing agents at low pressures evidently become highly effective at high pressures.

More than four-fifths of the world's historic gold production has come from mesothermal- and porphyry-type ore deposits (*1, 2*) in which aqueous fluids at temperatures (T) and pressures (P) well above the critical point of water are implicated in metal transport (*3*). Gold transport and deposition mechanisms in these deposits have been conjectural, largely because the fluid's gold-carrying capacity and identity of the dissolved gold species were undetermined at magmatic temperatures and contentious at 250° to 400°C. Here we report experimental identification of the gold solute species and solubility in supercritical fluids in the range of T and P in which hydrothermal fluids extract ore-forming solutes from granitoid magmas or rocks undergoing amphibolite- to granulite-facies metamorphism.

We isolated fluid samples from mineral reactants at the experimental T and P as large fluid inclusions ($\geq 75 \times 500$ μm) trapped in quartz in pits predrilled by laser ablation and sealed by quartz overgrowth during the experiment (*4*). The analysis used laser-ablation extraction of an individual fluid inclusion. The laser beam diameter was adjusted to include the immediately adjacent host quartz and so extract all quench precipitates in the inclusion. The ablation product was analyzed by inductively coupled plasma mass spectrometry (ICPMS) (*5*). Previous solubility studies with synthetic fluid inclusions used the precracked-quartz synthesis technique developed by Shelton and Orville (*6*) and were limited to ordinary microscope observation of thermally induced phase changes in solutions of extremely soluble salts (*7*). Quantitative measurement (to better than ±15%) of the solubilities of sparingly soluble solids in the tiny inclusions (typically <40 μm) produced by the cracked-quartz synthesis technique had to await development of sensitive ICPMS laser-ablation techniques (*8*).

In experiments assessing the role of Au-Cl species in sulfidic brine, we varied the chloride content in starting solutions at buffered activities of H^+, H_2, and H_2S, at constant

[1]Research School of Earth Sciences, [2]Department of Geology, Australian National University, Canberra, A.C.T. 0200, Australia.

*To whom correspondence should be addressed. E-mail: Robert.Loucks@anu.edu.au